



ELSEVIER

Contents lists available at ScienceDirect

## Applied Catalysis B: Environmental

journal homepage: www.elsevier.com



Research paper

Structural and electronic properties of oxygen defective and Se-doped *p*-type BiVO<sub>4</sub>(001) thin film for the applications of photocatalysis

Habib Ullah\*, Asif A. Tahir\*, Tapas K. Mallick

Environment and Sustainability Institute (ESI), University of Exeter, Penryn Campus, Penryn, Cornwall TR10 9FE, United Kingdom

## ARTICLE INFO

## Keywords:

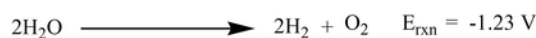
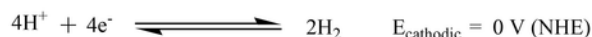
Se-doped BiVO<sub>4</sub>  
*p*-type semiconductor  
 Charge carriers  
 Water splitting

## ABSTRACT

Monoclinic BiVO<sub>4</sub> is being used as a photocatalyst due to its stability, cost-effectiveness, ease of synthesis, and narrow band gap. Although, the valence band maximum, VBM (~ -6.80 eV vs vacuum) of BiVO<sub>4</sub> is well below the redox potential of water but having less positive conduction band minimum, CBM (-4.56 eV vs vacuum), responsible for its low efficiency. We have carried out a comprehensive periodic density functional theory (DFT) simulations for the pristine, Oxygen defective (O<sub>v</sub>) and Se doped BiVO<sub>4</sub>, to engineer not only its CB edge position but the overall photocatalytic and charge carrier properties. Our theoretical method has nicely reproduced the experimental data of pristine BiVO<sub>4</sub>, which encouraged us to elaborate further its O<sub>v</sub> and Se-doped characteristics. It is found that both the O<sub>v</sub> (1% Oxygen vacancy) and Se-doped BiVO<sub>4</sub> (1–2% Se) have ideal band edges, band gaps, and small effective masses of electrons and holes, responsible for high photocatalytic activities. Moreover, Se-doped BiVO<sub>4</sub> behave as *p*-type semiconductor. Finally, the photocatalytic water-splitting behaviour of the selected surfaces were counterchecked with water interaction, where the strong water adsorption energy of about ~ -38 to -50 kcal/mol, confirms and predicts their higher efficiencies compared to that of parent BiVO<sub>4</sub>.

## 1. Introduction

Solar energy harnessing via photoelectrochemical (PEC) water splitting, using transition metal oxides, is a direct chemical energy conversion and storage technique. Since the discovery of the first photocatalytic water splitting experiment, a range of transition metal oxides have been employed to produce solar fuel [1]. An ideal photocatalyst must have valence band (VB) and conduction band (CB), which straddle the redox potentials of photocatalytic reaction, and must have high stability, availability, and narrow band gap which can absorb efficiently the visible part of sun light [2,3].



To date, the current focus semiconductors/photocatalysts are Fe<sub>2</sub>O<sub>3</sub>, LaFeO<sub>3</sub>, TaON, LaCrO<sub>3</sub>, LaCoO<sub>3</sub>, TiO<sub>2</sub>, BiVO<sub>4</sub>, ZnS, ZnO<sub>2</sub>, Bi<sub>2</sub>WO<sub>6</sub>, SrTiO<sub>3</sub>, BiOX (Cl, Br, I), and etc. Some of these semiconductors have ideal band edges position but they are either unstable or having large band gaps, while some of them are narrow band gap but one of the band edges (either VB or CB) is situated at improper band edge energy (see Scheme S1) [4]. So, the redox reaction cannot be completed without the external bias potential (see reactions 1–3). Band structure engineering is one of the excellent strategies to tailor the band edges and band gaps of these semiconductors, through doping process [5–7].

Bismuth vanadate (BiVO<sub>4</sub>) is a promising photocatalyst for solar energy conversion due to its nontoxic, low-cost, photostable, and eco-friendly nature. Generally, BiVO<sub>4</sub> has three different crystalline polymorphs: orthorhombic pucherite, tetragonal dreyerite, and monoclinic clinobisvanite [8]. These different polymorphs have different properties as the photocatalytic activity is strongly influenced by the crystal structure. For instance, the tetragonal BiVO<sub>4</sub> possesses a band gap of 2.9 eV and mainly absorbs UV region, while the monoclinic clinobisvanite (m-BiVO<sub>4</sub>) exhibits a much higher photocatalytic activity due to

\* Corresponding author.

Email address: habib\_chemist@yahoo.com (H. Ullah)

its ideal band gap (2.4–2.5 eV) which absorb the UV and visible regions of the electromagnetic spectrum, having an ideal valence band edge position for driving water oxidation [9]. However, it has been recently reported that m-BiVO<sub>4</sub>, an *n*-type semiconductor [10], exhibits poor photocatalytic property which is stem to low mobility of the photogenerated charge carriers (electron–hole pairs), positive potential of CB (vs NHE) and high charge recombination rates which significantly limit its practical applications. The photocatalytic activity of m-BiVO<sub>4</sub> can be tuned either with metal or non-metal doping, semi-conductor recombination (heterojunction formation), depositing the co-catalysts, defect formation (oxygen vacancy creation), and crystal-facet control or morphological modification.

Moreover, it is important to investigate/design an efficient dopant for BiVO<sub>4</sub>, which not only keeps its monoclinic crystal structure but to slow down the charge recombination rate and more negative CB (vs NHE) edge position. The monoclinic clinobisvanite structure of BiVO<sub>4</sub>, consists of rows of isolated [VO<sub>4</sub>] tetrahedra which are separated by the dodecahedral coordinated Bi atoms to form [BiO<sub>8</sub>] with eight O atoms (Fig. 1).

In order to improve the overall photocatalytic activity of m-BiVO<sub>4</sub> (simply denoted as BiVO<sub>4</sub>), different doping agents have been applied; these doping agents have either substituted the (I) V or (II) Bi atoms but no one has paid attention to substitute the (III) O site of BiVO<sub>4</sub>. The previous literature of different doping agents [11–18], used for BiVO<sub>4</sub> can be summarized as!

(I). Doping of BiVO<sub>4</sub> at the V-sites is very common but due to different valence states of the dopant, a distortion in the [VO<sub>4</sub>] tetrahedral chains cause phase transition from the parental monoclinic to tetragonal structure (Fig. 1). This distortion of [VO<sub>4</sub>] tetrahedron chains in BiVO<sub>4</sub>, plays a negative impact on the photocatalytic water-splitting, to generate H<sub>2</sub> gas. On the other hand, monoclinic BiVO<sub>4</sub> exhibits weak hole localization and is very helpful for water-splitting reaction. So, to keep the [VO<sub>4</sub>] tetrahedral in the monoclinic structure of BiVO<sub>4</sub>, Luo et al. have reported that ion doping with higher valence states such as Mo<sup>6+</sup> and W<sup>6+</sup>, to substitute V in BiVO<sub>4</sub>, not only keep the parental geometry but also enhanced its photocatalytic activity [19].

(II). Another useful dopant agent which keeps the tetrahedral geometrical part of [VO<sub>4</sub>] is Ce<sup>3+</sup>, which substitutes the Bi<sup>3+</sup> sites in BiVO<sub>4</sub>. Ce<sup>3+</sup> is a trivalent cation and has similar ionic radius to that of Bi<sup>3+</sup>, substitutes the Bi-sites and not the V-sites (V<sup>5+</sup>). Z. Jiang et al. have investigated that Ce<sup>3+</sup> ions doped-BiVO<sub>4</sub> (Ce-BiVO<sub>4</sub>) do not distort either the octahedral and dodecahedral geometries but act as trapping agent for the photogenerated holes which is responsible for the higher photocatalytic water oxidation activity compared to that of pristine one [20].

(III). No one has paid attention to substitute the O-sites in BiVO<sub>4</sub>, and we believe that its substitution with di-anionic species such as sele-

mium (Se<sup>2-</sup>), with appropriate amount of doping ratio, will not disturb both the [VO<sub>4</sub>] and [BiO<sub>8</sub>] geometries. Furthermore, Se<sup>2-</sup> would have dual attachment in the BiVO<sub>4</sub>, coordinated with Bi on one hand and with V on the other side.

In this work, we investigated the effect of Oxygen vacancy and Se-dopant for the geometrical structure and corresponding photocatalytic activity of BiVO<sub>4</sub>.

## 2. Computational methodology

First principle periodic boundary density functional theory (DFT) simulations are carried out, using Quantum ESPRESSO [21] and QuantumWise-ATK [22] while the results are visualized on VESTA [23] and vnl 2017.0 [24]. The experimentally observed crystallographic file of BiVO<sub>4</sub>; clinobisvanite structure is used as such which has Hall symmetry space group of I2/b with lattice parameters of  $a = 5.147 \text{ \AA}$ ,  $b = 5.147 \text{ \AA}$ ,  $c = 11.7216 \text{ \AA}$ , and  $\gamma = 90^\circ$  (See Fig. 1) [25]. Generalized gradient approximation (GGA) at Perdew-Burke-Ernzerhof (PBE) exchange-correlation functional is used for the structural and energy optimization [26]. As an input structure for the calculations; the 24 atoms primitive unit cell and its  $2 \times 2 \times 2$  supercell along with (001) direction with  $10 \text{ \AA}$  vacuum, is considered as a model for the periodic boundary condition (PBC) DFT simulations. The local density approximation (LDA) method is found to be superior in reproducing the experimental data of BiVO<sub>4</sub>, compared to pure GGA and meta GGA (MGGA). The detailed comparison of these methods is given in Supporting Information (Fig. S1 and S3). Generally, it is believed that clinobisvanite monoclinic BiVO<sub>4</sub> exists in (001) orientation so, that is why the (001) slab is opted for the theoretical simulations to represent its experimental thin film [27]. Moreover, the unreconstructed (001) termination possesses low surface energy and as a result represents the most probable surface termination [27]. Stability of these different slabs are confirmed from their positive formation energy and electrostatic potential; details of surface formation energy is give in Table S1 and Fig. S4-10 of the Supporting Information. A  $5 \times 5 \times 1$  Monkhorst-Pack k-grid and energy cutoff of 100 Ry is employed for the geometry relaxation and self-consistent (SCF) simulations of BiVO<sub>4</sub>; consisting of 96 atoms. The Broyden-Fletcher-Goldfarb-Shanno algorithm (BFGS) is used for the structural relaxation [28]. A  $5 \times 5 \times 5$  Monkhorst-Pack k-grid with the same energy cutoff is used for the non-SCF part to get the density of states (DOS) and partial DOS (PDOS). The band structure simulations were performed along the direction of  $\Gamma$ , Z, R, X, and M of the Brillouin zone. The valence electron configurations considered are:  $5d^{10} 6s^2 6p^3$  for Bi;  $3p^6 3d^3 4s^2$  for V;  $2s^2 2p^4$  for O,  $1s^2$  for H, and  $4s^2 4p^4 3d^{10}$  for Se atom.

## 3. Results and discussion

### 3.1. Optimized structures of pristine, oxygen defective, and Se-Doped BiVO<sub>4</sub>(001)

The removal of an oxygen atom, and Se dopant on the tetrahedral or dodecahedral geometries of monoclinic clinobisvanite is investigated from the resulting relaxed geometries. Optimized structures of these different species of BiVO<sub>4</sub> are given in Fig. 2, where the bond distances between V—O and Bi—O decrease; considering the case of O<sub>v</sub> and Se-doped BiVO<sub>4</sub>(001). When the Se dopant ratio is increased from 2 to 3 or 4, it distorted the geometries of parent BiVO<sub>4</sub>(001) as can be seen from Fig. 2. However, in case of 1–2% doping ratios, the resulted geometries were quite compact and similar to parent BiVO<sub>4</sub>(001).

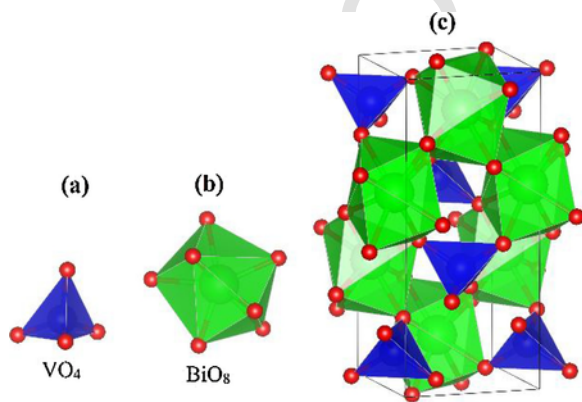


Fig. 1. Tetrahedral and dodecahedra geometries of VO<sub>4</sub> (a) and BiO<sub>8</sub> (b) in BiVO<sub>4</sub> (c).

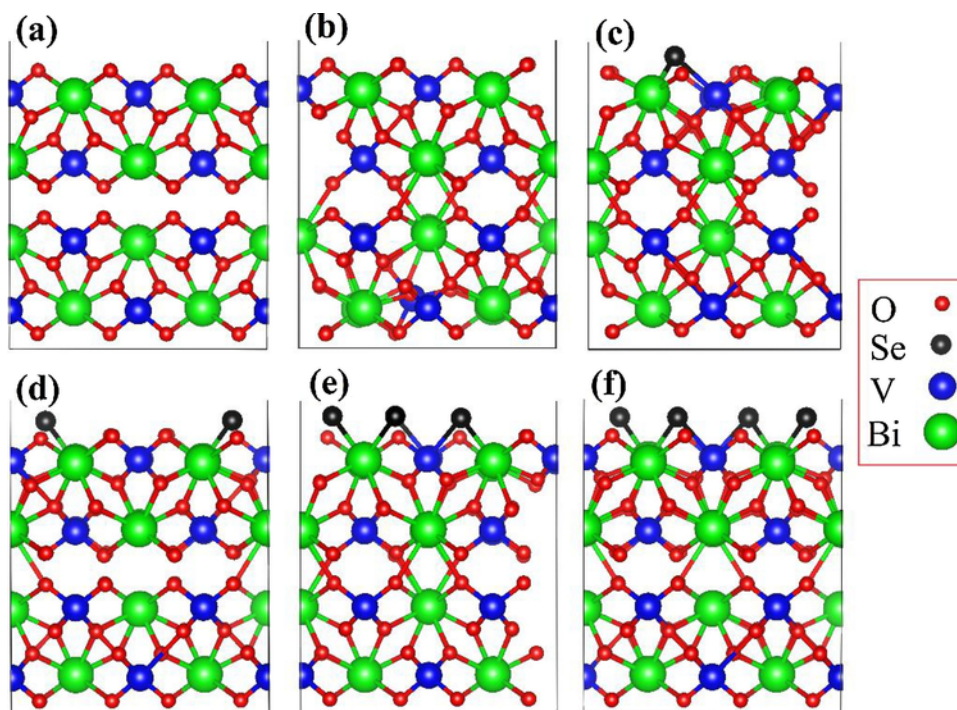


Fig. 2. Relaxed structures of (a)  $\text{BiVO}_4(001)$ , (b) Ov, (c) 1%, (d) 2%, (e) 3%, and (d) 4% Se doped  $\text{BiVO}_4(001)$ .

### 3.2. Electronic properties

#### 3.2.1. Electronic properties of $\text{BiVO}_4(001)$ surface

As discussed in our previous report [29], that the monoclinic clinobisvanite phase exhibits a much higher photocatalytic activity compared to its other polymorphs due to its favourable band gap (2.4–2.5 eV) in the visible region of electromagnetic spectrum and a valence band position suitable for driving water oxidation [9].

The electronic properties such as DOS/PDOS and band structure of  $\text{BiVO}_4(001)$  are given in Fig. 3, where its band gap is 2.24 eV. This band gap is about 0.16 eV smaller than that of experimental but it is expected from LDA [30], which underestimate the band gap. However, it has nicely reproduced both the VB and CB edge positions of pristine  $\text{BiVO}_4(001)$ ; ca. at  $-6.80$  eV and  $-4.56$  eV (vs vacuum), respectively. Analysis of the PDOS led us to conclude that orbitals of O atoms are responsible for developing valence band edge, however, the conduction band edge is that of V atoms. Contribution of the s, p, and d orbitals of Bi, V, and O, in making the band gap and edge positions are given in

Fig. S11 of the Supporting Information. The s and p orbitals of Bi atoms constitute VB and CB edge of Bi, 3d orbitals of V are responsible for its VB and CB while in case of O, 2p orbitals have a major role in developing their band edge positions. Band structure of the  $\text{BiVO}_4(001)$  along the k-points direction of  $\Gamma$ , Z, R, X, and M is given in Fig. 3, where an indirect band gap of 2.24 eV has good agreement with the experimental and recently theoretical reported data [9]. Furthermore, the simulated band edge energies (VBM  $\sim -6.80$  and CBM  $\sim -4.56$  eV at vacuum level) of  $\text{BiVO}_4$  indicate that its CBM need to be engineered for high PEC performance. The effective masses of the photogenerated electrons ( $m_e^*$ ) and holes ( $m_h^*$ ) along the  $X \rightarrow \Gamma$  directions of k-points are calculated by fitting parabolic approximation around the bottom of the CBM or the top of the VBM, respectively; using Eq. (1) (Table 1):

$$m^* = \hbar^2 (d^2 E/dk^2)^{-1} \quad (1)$$

where  $\hbar$  is the reduced Planck constant,  $E$  is the energy of an electron at wave vector  $k$  in the same band (VBM or CBM). The simulated values of the effective masses of photogenerated electrons and holes of the  $\text{BiVO}_4(001)$  are 0.09 and 0.28  $m_e$ , respectively.

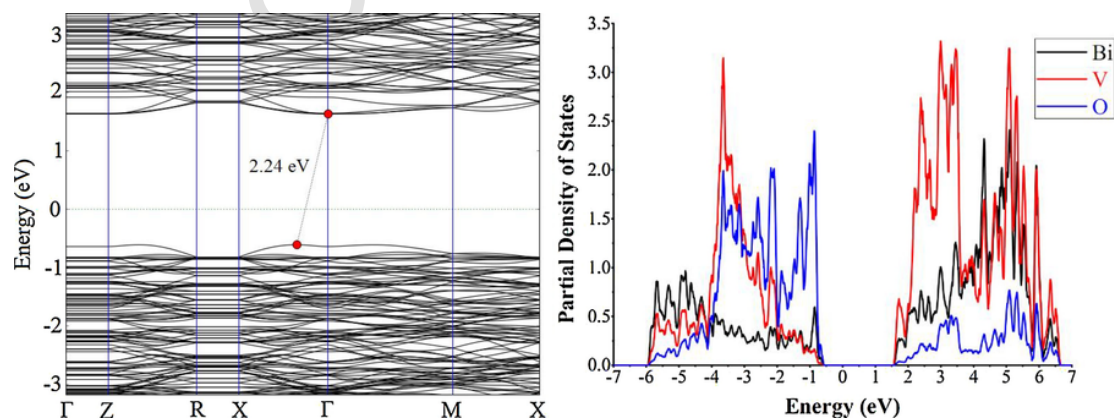


Fig. 3. Band Structure and PDOS plot of  $\text{BiVO}_4(001)$ ; the Fermi energy is set to zero.

**Table 1**  
Fermi energy, % doping, VBM, CBM, Band Gap, and Effective Masses of Photogenerated Electrons and Holes, Estimated from the calculated Band Structure along the suitable direction.

Species	Fermi Energy	% Doping	$m_e^*/m_0$	$m_h^*/m_0$	VBM	CBM	Band gap
BiVO <sub>4</sub> (001)	-6.18	Pure	0.09	0.28	-6.80	-4.56	2.24
O <sub>v</sub> -BiVO <sub>4</sub>	-4.28	1.0	0.19	0.18	-6.29	-4.33	1.96
1Se-BiVO <sub>4</sub> (001)	-5.17	1.04	0.09	0.02	-5.80	-4.41	1.39
2Se-BiVO <sub>4</sub> (001)	-5.19	2.08	0.04	0.31	-5.81	-4.08	1.73
3Se-BiVO <sub>4</sub> (001)	-4.93	3.0	0.65	2.02	-5.47	-4.39	1.08
4Se-BiVO <sub>4</sub> (001)	-4.73	4.16	0.01	0.24	-5.38	-4.14	1.24

The integrated local DOS (ILDOS) of BiVO<sub>4</sub>(001) within various energetic windows of the VBM, CBM, band gap, and electrostatic potential (ESP) are presented in Fig. 4. The ILDOS at the CBM (0–1.6 eV), as well as a cross section of the ILDOS through the (001) plane highlights the primary contribution from V orbitals which can be found from Fig. 3 and Fig. S11. Localization of CBM electrons is because of the poor hybridization of V neighbouring orbitals as can be seen from Figs. 3, 4 and S11. The poor photoelectrochemical performance BiVO<sub>4</sub> thin film can be correlated with poor hole mobility (effective mass of hole  $\sim 0.28 m_e$ ) rather than electron, which limits photocarrier transport and charge extraction. The self-trapping and small electron polaron formation in this material is due to the localization of photogenerated hole. Pristine BiVO<sub>4</sub>(001) is an *n*-type semiconductor where the electrons play an important role in the photocatalytic reaction. This statement also corroborate the already reported work of A. Rettie et al. [31] So, the relative delocalized orbitals at CBM compared to VBM (Fig. 3) confirmed that majority of hole, limit the charge transport in this material.

### 3.3. Electronic properties of oxygen vacancy BiVO<sub>4</sub>(001) surface

In order to understand the effect of oxygen vacancy (O<sub>v</sub>) on the photoelectrochemical performance of BiVO<sub>4</sub>, 1% O<sub>v</sub>-BiVO<sub>4</sub>(001) is employed for DFT simulations. The VB and CB orbitals distributions are almost similar to that of parent slab, however, the Fermi energy merge in the CB which is due to the extra electron(s) of the O<sub>v</sub>, as can be seen from Fig. 5. It is also reported that monoclinic BiVO<sub>4</sub> is normally an intrinsic *n*-type semiconductor [32]. The contribution of V, Bi, and O orbitals are comparatively given in Fig. S12 of the Supporting Information. In this case, the electrons (0.19  $m_e$ ) are said to be the “majority carriers” for current flow (behave as an *n*-type semiconductor) while the effective mass of holes is 0.18  $m_e$ . Overall, small effective masses of electrons and holes are estimated from the CBM and VBM of O<sub>v</sub>-BiVO<sub>4</sub>(001) compared to that of parent slab. At vacuum level, the CBM and VBM are -6.29 and -4.33 eV, which are well above and below the redox potential of water, respectively (Table 1). Moreover, electron doping (Oxygen vacancy creation) of BiVO<sub>4</sub> has not only re-

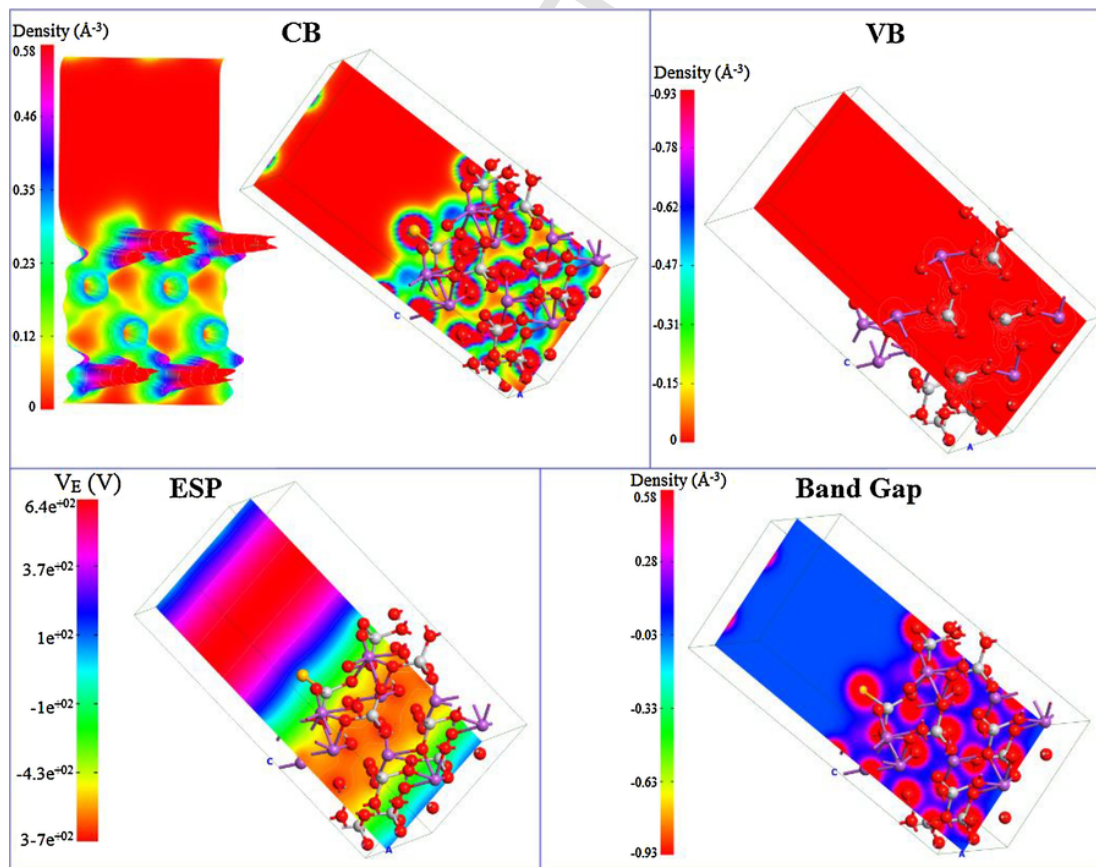


Fig. 4. Integrated local density of states of CBM, VBM, Band gap and ESP of BiVO<sub>4</sub>(001).

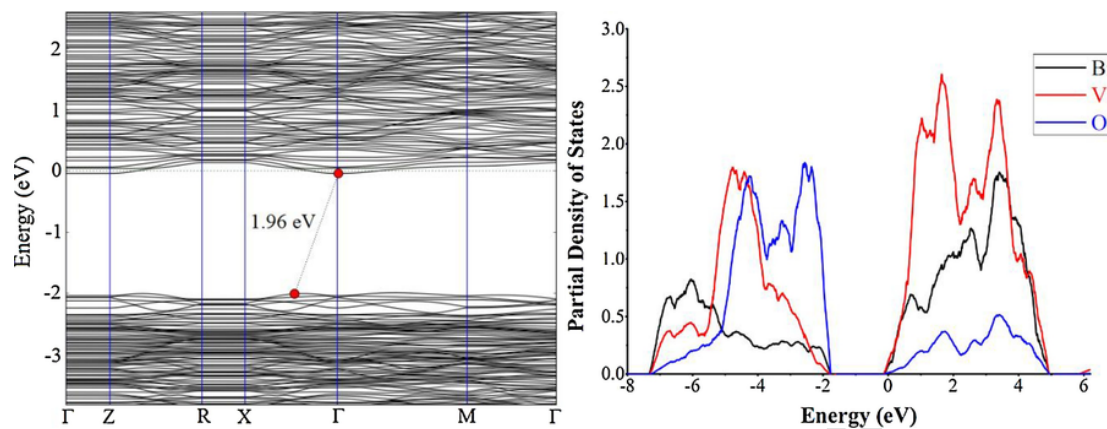


Fig. 5. Band Structure and PDOS plot of  $O_v\text{-BiVO}_4(001)$ ; the Fermi energy is set to zero.

duced its band gap, but shift the CB to more positive potential (vs vacuum) as can be seen from Table 1.

### 3.4. Electronic properties of Se-Doped $\text{BiVO}_4(001)$ surfaces

In order to improve the photocatalytic performance of  $\text{BiVO}_4$ , Se is incorporated in the form of different dopant concentrations. Oxygen atom(s) is substituted with Se in  $\text{BiVO}_4(001)$ , from 1 to 4% dopant ratios, denoted as 1Se, 2Se, 3Se and 4Se- $\text{BiVO}_4(001)$ . 1% Se-doped has excellently improved the visible light absorption of  $\text{BiVO}_4(001)$  as can be seen from its band gap reduction, from 2.24 to 1.39 eV (Fig. 6 and Table 1). Moreover, p orbitals of Se constitute the VB of 1Se- $\text{BiVO}_4(001)$ , as can be seen from its PDOS plot (Fig. 6). The individual PDOS plots of Bi, V, O, and Se are shown in Fig. S13 of the Supporting Information. Se has not only reduced the band gap of parent  $\text{BiVO}_4$ , but changed both the VB and CB, to  $-5.80$  eV and  $-4.41$  eV (vs vacuum), respectively. Compared to parent  $\text{BiVO}_4(001)$ , 1Se- $\text{BiVO}_4(001)$  has an ideal CBM position which is well above the redox potential of water, responsible for water reduction. Se is a p-type dopant, which has produced some flat bands in the VB of parent  $\text{BiVO}_4(001)$ , however, it has significantly reduced the effective masses of electrons and holes (Table 1). The effective masses of these photocarriers are  $0.09 m_e$  for electron and  $0.02 m_e$  of hole (Note: for the effective masses of hole, we considered the third band, below the VBM). On the other hand, flat band of VB produces an effective mass of holes of about  $7.12 m_e$ , which are responsible for stationary holes. In summary, the high DOS in the VB Fermi level shift towards CB is clear evidence of the p-type nature of 1Se- $\text{BiVO}_4(001)$ . Moreover, 1Se- $\text{BiVO}_4(001)$  can be used as a best photocatalyst for solar water splitting due to its ideal band edges positions, narrow band gap, and small effective masses of charge carriers (*vide infra*).

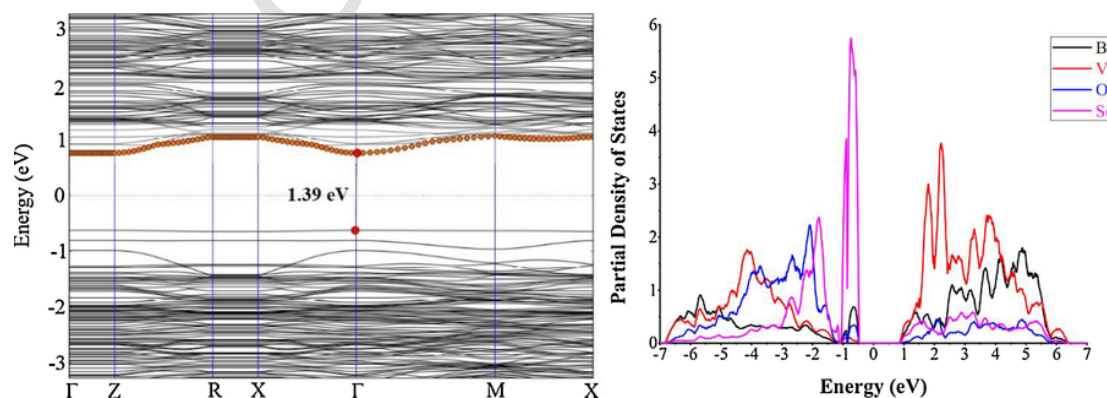


Fig. 6. Band structure and PDOS of 1% Se- $\text{BiVO}_4(001)$ ; the Fermi energy is set to zero.

In the searching of an optimum dopant ratio of Se, to design an efficient photocatalyst, we also considered the 2Se- $\text{BiVO}_4(001)$  system. The simulated band structure and PDOS of 2Se- $\text{BiVO}_4(001)$  are given in Fig. 7, while its comparative PDOS plot for Bi, V, O, and Se atoms are given in Fig. S14 of the Supporting Information. Again, the VB and CB are made of Se and V atoms, respectively. The VB and CB of 2Se- $\text{BiVO}_4(001)$  are situated at  $-5.81$  and  $-4.08$  eV (at vacuum), respectively which result band gap of 1.73 eV. Moreover, the simulated effective masses of electrons and holes are  $0.04 m_e$  and  $0.31 m_e$ , respectively, which predict high carrier mobility and charge separation rate. Very similar to 1Se- $\text{BiVO}_4(001)$ , 2Se- $\text{BiVO}_4(001)$  also behave as a p-type semiconductor as can be seen from its band structure and PDOS plot. So, both the 1 and 2% Se doped  $\text{BiVO}_4(001)$  have almost similar photocatalytic characteristics and can be used for efficient water splitting, especially for water reduction.

The effect of 3 and 4% Se on  $\text{BiVO}_4(001)$  and their band gap and effective masses of charge carriers are contrast to that of 1 and 2%, as can be seen from Table 1 and Fig. 8. For simplicity reason, the band gap and orbitals contribution of Bi, V, O, and Se of 3 and 4% Se-doped  $\text{BiVO}_4(001)$  are given in Fig. S15-S18 of the Supporting Information. Although, this higher doping concentration has well reduced the bandgap of parent  $\text{BiVO}_4(001)$ , 1.08 eV for 3 and 1.24 eV for 4% Se, but on the other hand it has sufficiently increased the VB and CB values (vs vacuum). The CBM positions of both these systems is well above the redox potential of water (vs vacuum) but the VBM is not able to perform the oxidation of water, to complete the overall water splitting reaction. The VBM and CBM of 3Se- $\text{BiVO}_4(001)$  are  $-5.47$  and  $-4.39$  eV while that of 4Se- $\text{BiVO}_4(001)$  are  $-5.38$  and  $-4.14$  eV, respectively. For the effective masses of charge carriers of these two systems, see Table 1.

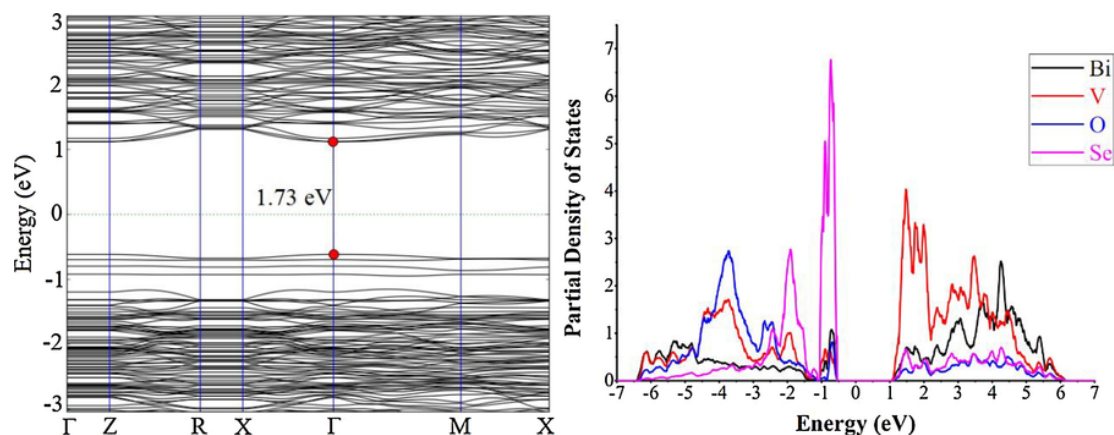


Fig. 7. Band Structure and PDOS plot of 2% Se:BiVO<sub>4</sub>(001); the Fermi energy is set to zero.

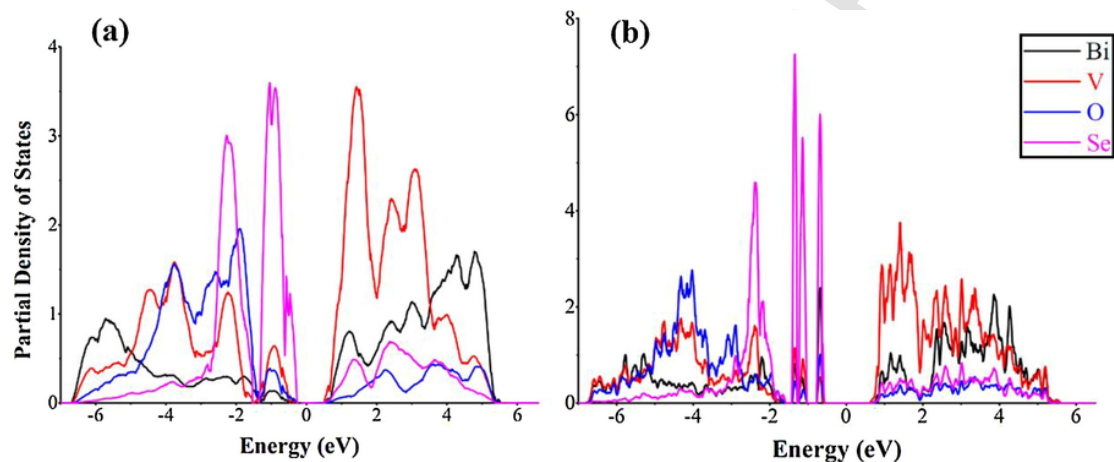


Fig. 8. PDOS plot of (a) 3Se and (b) 4Se:BiVO<sub>4</sub>(001); the Fermi energy is set to zero.

Comparative analysis of the Oxygen defective and Se doped (1–4%) BiVO<sub>4</sub>(001), led us to conclude that both the defective and mild (1 and 2%) Se-Doped BiVO<sub>4</sub>(001) are best candidates for photocatalytic water splitting, based on their simulated VB, CB, Bandgap and effective masses of charge carriers.

### 3.5. Adsorption of water on pristine, oxygen defective, and 1% Se doped BiVO<sub>4</sub>(001)

In order to elaborate the photocatalytic performance of the titled species, we adsorb water molecules on the surface of pristine, O<sub>v</sub>- and 1Se:BiVO<sub>4</sub>(001), see Fig. 9 for their relaxed structures. Two molecules of water are adsorbed on each of these surfaces, optimized and followed by electronic properties simulations such as bandgap, band edge and effective masses of charge carriers. The adsorption energy of water

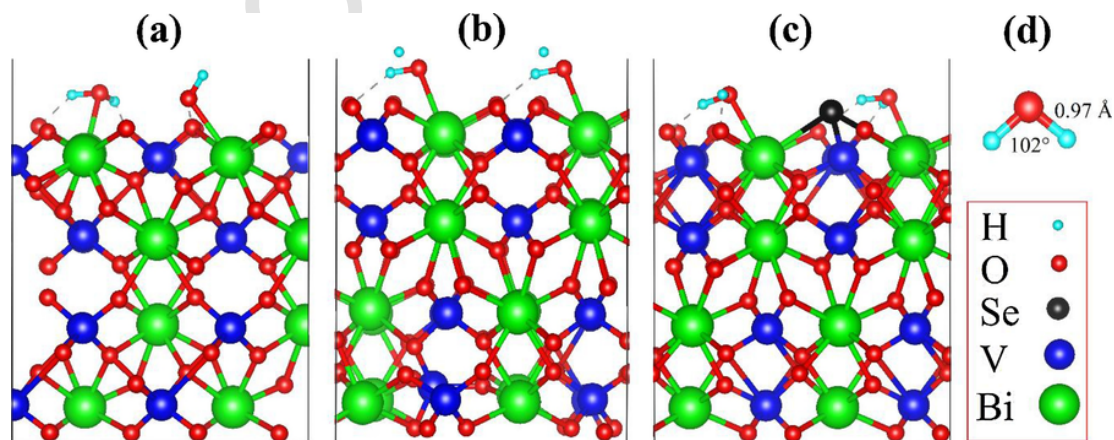


Fig. 9. Relaxed structure of (a) BiVO<sub>4</sub>(001)@H<sub>2</sub>O, (b) O<sub>v</sub>-BiVO<sub>4</sub>(001)@H<sub>2</sub>O, (c) 1Se:BiVO<sub>4</sub>(001)@H<sub>2</sub>O, and (d) water.

**Table 2**  
Inter-bond distance, Water Adsorption Energy ( $E_{ad}$ ), and Bandgaps of Water Adsorbed-BiVO<sub>4</sub>(001), Ov, and 1Se\_BiVO<sub>4</sub>(001) Systems.

Species	$H_{(water)}-O_{(surface)}$ (Å)	$Bi_{(surface)}-O_{(water)}$ (Å)	$E_{ad}$ (kcal/mol)	Band gap
BiVO <sub>4</sub> (001)@H <sub>2</sub> O	1.62	2.45	-38.28	1.74
O <sub>v</sub> _BiVO <sub>4</sub> @H <sub>2</sub> O	1.75	2.51	-50.85	2.28
1Se_BiVO <sub>4</sub> @H <sub>2</sub> O	1.59	2.45	-40.24	1.35

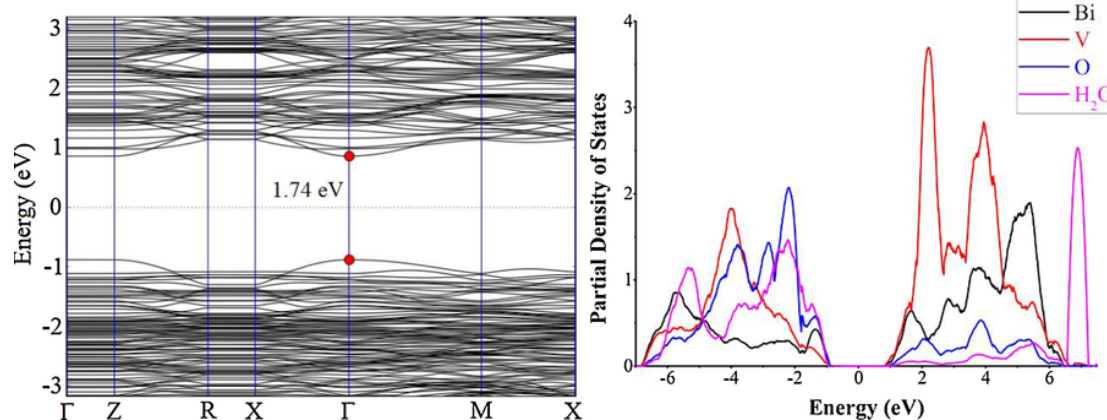


Fig. 10. Band Structure and PDOS plot of BiVO<sub>4</sub>-001@H<sub>2</sub>O; the Fermi energy is set to zero.

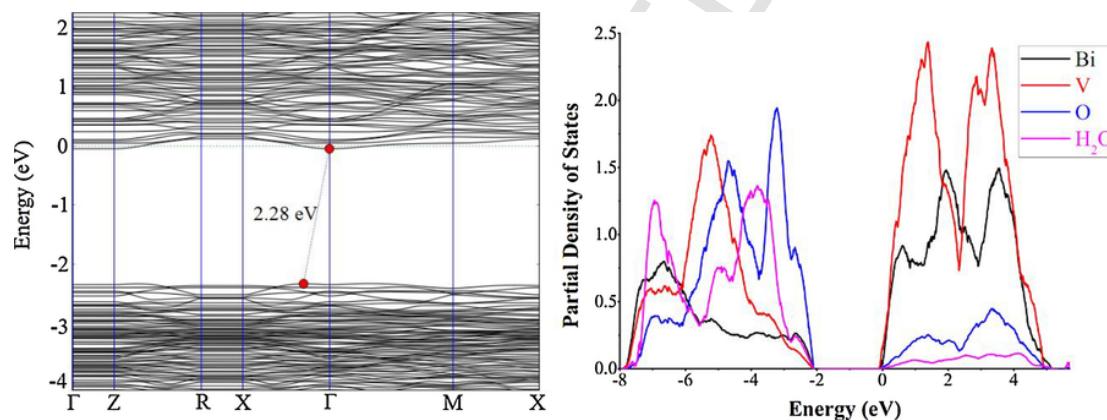


Fig. 11. Band structure and PDOS of O<sub>vac</sub>-BiVO<sub>4</sub>(001)@H<sub>2</sub>O; the Fermi energy is set to zero.

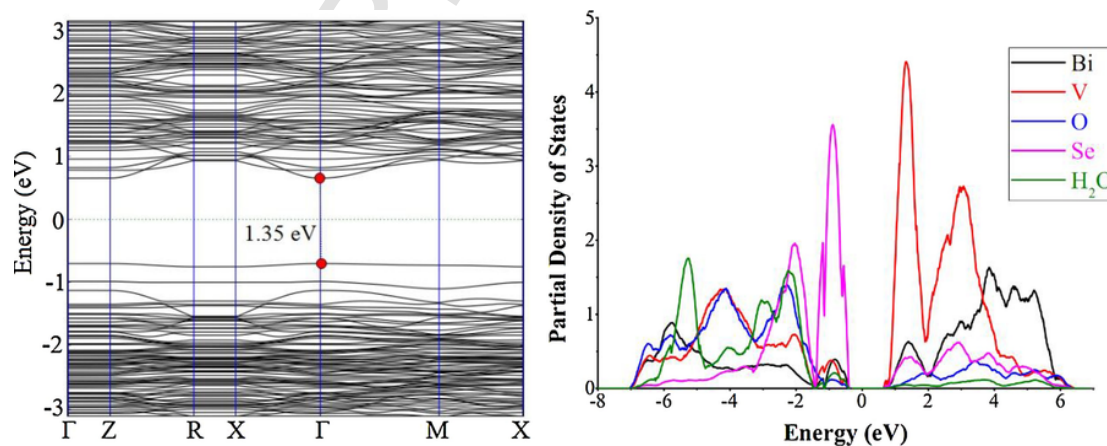


Fig. 12. Band structure and PDOS of 1Se-BiVO<sub>4</sub>(001)@H<sub>2</sub>O; the Fermi energy is set to zero.

molecules is simulated with the help of Eq. (1), by subtracting the energies of the optimized water molecule and adsorbent bare slab ( $E_{\text{slab}}$ ) from the optimized water-slab complex (slab@water), using Eq. (1).

$$\Delta E_{\text{ad}} = E_{\text{slab@water}} - (E_{\text{water}} + E_{\text{slab}}) \quad (1)$$

### 3.6. Pristine BiVO<sub>4</sub>(001)@H<sub>2</sub>O

In case of BiVO<sub>4</sub>(001)@H<sub>2</sub>O, one of the water molecules is more attracted towards the surface via O—Bi and two H—O bondings, having distances of 2.45 and 1.62 Å, respectively (Table 2).

Hydrogen atoms of water molecules make a strong hydrogen bonding with the surface O atoms of BiVO<sub>4</sub>(001), consequences the water splitting ability of pristine BiVO<sub>4</sub>. The parent H—O bond distances (0.97 Å) and H—O—H angle (102°) of water molecule enlarged to 1 Å and 110.41°, respectively when H<sub>2</sub>O is adsorbed on the (001) surface of BiVO<sub>4</sub>. The per-water molecular adsorption energy is −38.28 kcal/mol, responsible for H<sub>2</sub>O splitting over (001) surface of BiVO<sub>4</sub>. Moreover, the negative  $\Delta E_{\text{ad}}$  value indicates an exothermic adsorption process.

The electronic band structure and PDOS plot of BiVO<sub>4</sub>(001)@H<sub>2</sub>O are given in Fig. 10, where the band gap of parent BiVO<sub>4</sub>(001) is reduced to 1.74 eV upon adsorption of water molecules. So, the bandgap reduction of 0.48 eV confirm the water affinity of BiVO<sub>4</sub> towards its (001) surface. From the band structure and PDOS (Fig. 10) of BiVO<sub>4</sub>(001)@H<sub>2</sub>O system, it can be concluded that the VB orbital of water molecules has strong hybridization with the VB of BiVO<sub>4</sub>(001). Comparative analysis of the data of Table 1 and Fig. 10, led us to conclude that the water has moved the VB of pristine BiVO<sub>4</sub>(001) from −6.80 to −5.96 eV and CB from −4.56 to −4.22 eV, at vacuum level. The individual PDOS plots of Bi, V, O, and H<sub>2</sub>O is given in Fig. S19 of the Supporting Information. In summary, the strong adsorption energy, perturbation in both inter, and intra-bond distances of water and BiVO<sub>4</sub>(001), confirmed and validate the already experimental photocatalytic ability of BiVO<sub>4</sub> [33,34].

### 3.7. Oxygen defective BiVO<sub>4</sub>(001)@H<sub>2</sub>O

As discussed earlier, the Oxygen defective BiVO<sub>4</sub>(001) has ideal band edge positions (well above and below the redox potential of water) and narrow band gap to be used as photocatalyst for water splitting. This defective surface has strong attraction for water molecules as can be observed from its adsorption energy (−50.85 kcal/mol). However, the inter-bond distances of H—O and Bi—O are longer compared to that of pristine@H<sub>2</sub>O system. The reason behind this is, the more electropositive nature of O<sub>v</sub>-BiVO<sub>4</sub>(001) surface (especially O and Bi atoms), results weak hydrogen and electrostatic type of bondings (Table 2). In O<sub>v</sub>-BiVO<sub>4</sub>(001), the H—O bond distances of water molecules elongate to 0.99 Å, which result its further dissociation, as can be seen from Fig. 9b. The inter-bond distances such as the H—O (H of water and O of surface) are became enlarged which can be regarded to the cationic nature of O defective surface of BiVO<sub>4</sub>(001).

Upon adsorption of water molecules on the Oxygen defective surface, the band gap of the resulted specie increases from 1.96 to 2.28 eV, as can be seen from Fig. 11 and Table 1 and 2. This 0.32 eV bandgap enlargement is due to the shifting of CB, which is about 0.38 eV compared to parent slab as can be seen from the PDOS of O<sub>v</sub>-BiVO<sub>4</sub>(001). Contrast to BiVO<sub>4</sub>(001)@H<sub>2</sub>O system, here water molecules has sufficiently changed the energy of CB of O<sub>v</sub>-BiVO<sub>4</sub>(001). The strong interaction of water with the O defective surface can be analysed from its highest adsorption energy (−50.85 kcal/mol) and orbital overlapping, especially in the VB of O<sub>v</sub>-BiVO<sub>4</sub>(001)@H<sub>2</sub>O system (Fig. 11). The individual PDOS plots of Bi, V, O, and H<sub>2</sub>O are given in Fig. S20 of the Supporting Information.

### 3.8. 1% Se-Doped-BiVO<sub>4</sub>(001)@H<sub>2</sub>O

Finally, the water adsorption on the 1Se-BiVO<sub>4</sub>(001) surface is investigated, where its optimized parameters are given in Table 2 and electronic properties in Fig. 12 and S21. The simulated water adsorption energy (−40.24 kcal/mol) led us to conclude that 1% Se doped BiVO<sub>4</sub>(001) can be easily used an efficient photocatalytic material. Furthermore, the inter-Hydrogen bonding and electrostatic bond distances are 1.59 and 2.45 Å, respectively, which confirm the enhanced catalytic ability of Se doped BiVO<sub>4</sub>. Besides these geometric parameters, electronic properties of the resulting system are also effected, upon adsorption of water molecules. Both the VB and CB are slightly moved from its parental position, which has decreased the overall band gap, from 1.39 to 1.35 eV as can be seen from Fig. 12 and Table 2.

In summary, although pristine BiVO<sub>4</sub> is a good photocatalyst for water splitting, having narrow bandgap and VB edge position, but inappropriate CB potential, reduces its hydrogen evaluation efficiency. This comprehensive theoretical simulation predicts that both the Oxygen defective and mild doped (1 or 2% Se) BiVO<sub>4</sub> have not only changed the band edges positions (well above and below the redox potential of water) but reduced the bandgap as well, results a champion photocatalyst for water splitting.

## 4. Conclusion

We have carried out a comprehensive periodic density functional theory (DFT) simulations for the pristine, oxygen defective (O<sub>v</sub>) and Se-doped BiVO<sub>4</sub>(001), to improve its photocatalytic performance. BiVO<sub>4</sub> is a stable, cheap, easily synthesizable, having appropriate band gap and valance band (VB) edge position but less positive conduction band (CB) edge position (vs vacuum). Our theoretical simulations of BiVO<sub>4</sub>(001) surface has nicely reproduced the experimental data which has validated and confirm the method used. Furthermore, it is found that O<sub>v</sub> (1%), and Se-doped (1–2%) BiVO<sub>4</sub>(001) have narrowed band gaps, small effective masses of electrons and holes, and well above and below CBM and VBM, respectively (in line with the redox potential of water). Moreover, Se-doped BiVO<sub>4</sub>(001) behave as a *p*-type semiconductor, capable of H<sub>2</sub> production from water reduction. Finally, the selected surfaces were interacted with water molecules, to check their water absorption energy. The water adsorption energies vary as O<sub>v</sub>-BiVO<sub>4</sub>(001)@H<sub>2</sub>O > 1Se-BiVO<sub>4</sub>(001)@H<sub>2</sub>O > BiVO<sub>4</sub>(001)@H<sub>2</sub>O. Although, Oxygen defective (1% O vacancy) BiVO<sub>4</sub>(001) has narrow band gap (1.96 eV), suitable redox potentials (VB −6.29 eV, CB −4.33 eV at vacuum level), and high-water adsorption energy but thermodynamically less stable compared to Se-doped BiVO<sub>4</sub>(001). So, we conclude and predict that mild doped Se-BiVO<sub>4</sub>(001) is not only stable but can efficiently absorb the visible part of sun light and split water into O<sub>2</sub> and H<sub>2</sub> without any external biased.

## Acknowledgment

We acknowledge the supercomputing facilities of ESI Beowulf Cluster, University of Exeter, UK.

## Appendix A. Supplementary data

Supplementary data associated with this article can be found, in the online version, at <https://doi.org/10.1016/j.apcatb.2017.11.034>.

## References

- [1] A. Fujishima, Electrochemical photolysis of water at a semiconductor electrode, *Nature* 238 (1972) 37–38.



- [2] M.G. Walter, E.L. Warren, J.R. McKone, S.W. Boettcher, Q. Mi, E.A. Santori, N.S. Lewis, Solar water splitting cells, *Chem. Rev.* 110 (2010) 6446–6473.
- [3] T. Hisatomi, J. Kubota, K. Domen, Recent advances in semiconductors for photocatalytic and photoelectrochemical water splitting, *Chem. Soc. Rev.* 43 (2014) 7520–7535.
- [4] J. Li, N. Wu, Semiconductor-based photocatalysts and photoelectrochemical cells for solar fuel generation: a review, *Catal. Sci. Technol.* 5 (2015) 1360–1384.
- [5] H. Ullah, Inter-molecular interaction in Polypyrrole/TiO<sub>2</sub>: a DFT study *J. Alloys Compd.* 692 (2017) 140–148.
- [6] H. Ullah, A.A. Tahir, T.K. Mallick, Polypyrrole/TiO<sub>2</sub> composites for the application of photocatalysis, *Sens. Actuators B* 241 (2017) 1161–1169.
- [7] X. Jia, J. Cao, H. Lin, M. Zhang, X. Guo, S. Chen, Transforming type-I to type-II heterostructure photocatalyst via energy band engineering: a case study of I-BiOCl/I-BiOBr, *Appl. Catal. B: Environ.* 204 (2017) 505–514.
- [8] M.D. Rossell, P. Agrawal, A. Borgschulte, C. c. Hébert, D. Passerone, R. Erni, Direct evidence of surface reduction in monoclinic BiVO<sub>4</sub>, *Chem. Mater.* 27 (2015) 3593–3600.
- [9] H.S. Park, K.E. Kweon, H. Ye, E. Paek, G.S. Hwang, A.J. Bard, Factors in the metal doping of BiVO<sub>4</sub> for improved photoelectrocatalytic activity as studied by scanning electrochemical microscopy and first-principles density-functional calculation, *J. Phys. Chem. C* 115 (2011) 17870–17879.
- [10] M. Long, W. Cai, H. Kisch, Visible light induced photoelectrochemical properties of n-BiVO<sub>4</sub> and n-BiVO<sub>4</sub>/p-Co<sub>3</sub>O<sub>4</sub>, *J. Phys. Chem. C* 112 (2008) 548–554.
- [11] S.K. Cho, H.S. Park, H.C. Lee, K.M. Nam, A.J. Bard, Metal doping of BiVO<sub>4</sub> by composite electrodeposition with improved photoelectrochemical water oxidation, *J. Phys. Chem. C* 117 (2013) 23048–23056.
- [12] S.K. Pilli, T.E. Furtak, L.D. Brown, T.G. Deutsch, J.A. Turner, A.M. Herring, Cobalt-phosphate (Co-Pi) catalyst modified Mo-doped BiVO<sub>4</sub> photoelectrodes for solar water oxidation, *Energy Environ. Sci.* 4 (2011) 5028–5034.
- [13] X. Zhang, Y. Zhang, X. Quan, S. Chen, Preparation of Ag doped BiVO<sub>4</sub> film and its enhanced photoelectrocatalytic (PEC) ability of phenol degradation under visible light, *J. Hazard. Mater.* 167 (2009) 911–914.
- [14] C. Yin, S. Zhu, Z. Chen, W. Zhang, J. Gu, D. Zhang, One step fabrication of C-doped BiVO<sub>4</sub> with hierarchical structures for a high-performance photocatalyst under visible light irradiation, *J. Mater. Chem. A* 1 (2013) 8367–8378.
- [15] S. Obregón, G. Colón, Heterostructured Er<sup>3+</sup> doped BiVO<sub>4</sub> with exceptional photocatalytic performance by cooperative electronic and luminescence sensitization mechanism, *Appl. Catal. B* 158 (2014) 242–249.
- [16] M. Wang, Q. Liu, Y. Che, L. Zhang, D. Zhang, Characterization and photocatalytic properties of N-doped BiVO<sub>4</sub> synthesized via a sol-gel method, *J. Alloys Compd.* 548 (2013) 70–76.
- [17] G. Tan, L. Zhang, H. Ren, J. Huang, W. Yang, A. Xia, Microwave hydrothermal synthesis of N-doped BiVO<sub>4</sub> nanoplates with exposed (040) facets and enhanced visible-light photocatalytic properties, *Ceram. Int.* 40 (2014) 9541–9547.
- [18] W.J. Jo, J.W. Jang, K. j. Kong, H.J. Kang, J.Y. Kim, H. Jun, K. Parmar, J.S. Lee, Phosphate doping into monoclinic BiVO<sub>4</sub> for enhanced photoelectrochemical water oxidation activity, *Angew. Chem. Int. Ed.* 51 (2012) 3147–3151.
- [19] W. Luo, J. Wang, X. Zhao, Z. Zhao, Z. Li, Z. Zou, Formation energy and photoelectrochemical properties of BiVO<sub>4</sub> after doping at Bi<sup>3+</sup> or V<sup>5+</sup> sites with higher valence metal ions, *Phys. Chem. Chem. Phys.* 15 (2013) 1006–1013.
- [20] Z. Jiang, Y. Liu, T. Jing, B. Huang, X. Zhang, X. Qin, Y. Dai, M.-H. Whangbo, Enhancing the photocatalytic activity of BiVO<sub>4</sub> for oxygen evolution by ce doping: Ce<sup>3+</sup> ions as hole traps, *J. Phys. Chem. C* 120 (2016) 2058–2063.
- [21] P. Giannozzi, S. Baroni, N. Bonini, M. Calandra, R. Car, C. Cavazzoni, D. Ceresoli, G.L. Chiarotti, M. Cococcioni, I. Dabo, QUANTUM ESPRESSO: a modular and open-source software project for quantum simulations of materials, *J. Phys. Condens. Matter* 21 (2009) 395502.
- [22] Atomistix ToolKitversion. 0, QuantumWise A/S, 2017, ([www.quantumwise.com](http://www.quantumwise.com)).
- [23] K. Momma and F. Izumi, An integrated three-dimensional visualization system VESTA using wxWidgets Commision Crystallogr. Comput., *IUCr Newslett.* 2006. 106–119.
- [24] Virtual NanoLabversion.0, QuantumWise A/S, 2017 ([www.quantumwise.com](http://www.quantumwise.com)).
- [25] A. Sleight, H.-Y. Chen, A. Ferretti, D. Cox, Crystal growth and structure of BiVO<sub>4</sub>, *Mater. Res. Bull.* 14 (1979) 1571–1581.
- [26] A.H. Larsen, M. Vanin, J.J. Mortensen, K.S. Thygesen, K.W. Jacobsen, Localized atomic basis set in the projector augmented wave method, *Phys. Rev. B* 80 (2009) 195112.
- [27] G. Xi, J. Ye, Synthesis of bismuth vanadate nanoplates with exposed {001} facets and enhanced visible-light photocatalytic properties, *Chem. Commun.* 46 (2010) 1893–1895.
- [28] W.H. Press, Numerical recipes, The Art of Scientific Computing, 3rd edition, Cambridge University Press, 2007.
- [29] S.N.F.M. Nasir, H. Ullah, M. Ebadi, A.A. Tahir, J.S. Sagu, M.A. Mat Teridi, New insights into Se/BiVO<sub>4</sub> heterostructure for photoelectrochemical water splitting: a combined experimental and DFT study, *J. Phys. Chem. C* 121 (2017) 6218–6228.
- [30] F. Tran, P. Blaha, Accurate band gaps of semiconductors and insulators with a semilocal exchange-correlation potential, *Phys. Rev. Lett.* 102 (2009) 226401.
- [31] A.J. Rettie, H.C. Lee, L.G. Marshall, J.-F. Lin, C. Capan, J. Lindemuth, J.S. McCloy, J. Zhou, A.J. Bard, C.B. Mullins, Combined charge carrier transport and photoelectrochemical characterization of BiVO<sub>4</sub> single crystals: intrinsic behavior of a complex metal oxide, *J. Am. Chem. Soc.* 135 (2013) 11389–11396.
- [32] Z. He, Y. Shi, C. Gao, L. Wen, J. Chen, S. Song, BiOCl/BiVO<sub>4</sub> p-n heterojunction with enhanced photocatalytic activity under visible-light irradiation, *J. Phys. Chem. C* 118 (2013) 389–398.
- [33] D. Wang, R. Li, J. Zhu, J. Shi, J. Han, X. Zong, C. Li, Photocatalytic water oxidation on BiVO<sub>4</sub> with the electrocatalyst as an oxidation cocatalyst: essential relations between electrocatalyst and photocatalyst, *J. Phys. Chem. C* 116 (2012) 5082–5089.
- [34] S. Sun, W. Wang, D. Li, L. Zhang, D. Jiang, Solar light driven pure water splitting on quantum sized BiVO<sub>4</sub> without any cocatalyst, *ACS Catal.* 4 (2014) 3498–3503.